Title

Lithium Insertion Processes of Orthorhombic Na{sub x}MnO{sub 2}-based Electrode Materials

Author

Doeff, M.M.

Publication Date

1995-12-01

LBL-38069
UC-404
Preprint

Lawrence Berkeley Laboratory
UNIVERSITY OF CALIFORNIA

Materials Sciences Division

Submitted to Journal of the Electrochemical Society

Lithium Insertion Processes of Orthorhombic Na_xMnO_2-based Electrode Materials

M.M. Doeff, T.J. Richardson, and L. Kepley

December 1995

Prepared for the U.S. Department of Energy under Contract Number DE-AC03-76SF00098

DISCLAIMER

LBL-38069
UC-404

Lithium Insertion Processes of Orthorhombic Na_xMnO_2-based Electrode Materials

Marca M. Doeff, Thomas J. Richardson, and Larry Kepley

Materials Sciences Division
Lawrence Berkeley National Laboratory
University of California
Berkeley, California 94720

December 1995

This work was supported by the United States Advanced Battery Consortium (USABC) under a Cooperative Research and Development Agreement with the Ernest Orlando Lawrence Berkeley National Laboratory. The USABC is a partnership of Chrysler, Ford, and General Motors, with technical and financial participation of the Electric Power Research Institute (EPRI)/utilities and the United States Department of Energy, under Contract No. DE-AC03-76SF00098.

Lithium Insertion Processes of Orthorhombic Na_xMnO_2-based Electrode Materials

Marca M. Doeff, Thomas J. Richardson and Larry Kepley

Materials Sciences Division
Lawrence Berkeley National Laboratory
University of California
Berkeley, CA 94720

Acknowledgment: This work was supported by the United States Advanced Battery Consortium (USABC) under a cooperative research and development agreement with the Lawrence Berkeley Laboratory. The USABC is a partnership of Chrysler, Ford and General Motors, with technical and financial participation of the Electric Power Research Institute (EPRI)/utilities and the United States Department of Energy. The program manager for this work is Dr. Robert Swaroop.

Abstract

Electrochemical, thermal and structural characterization of lithium insertion processes into orthorhombic Na_xMnO_2-based materials is presented. "Chimie douce" oxidation, reduction and/or exchange reactions of the precursor $Na_{0.44}MnO_2$ can be used to prepare high capacity (180 mAh/g), high voltage compounds for use in secondary lithium batteries. Lithiated Na_xMnO_2 is quite stable; formation of the thermodynamically favored tetragonally distorted spinel, $Li_{1+x}Mn_2O_4$, occurs only under conditions of prolonged severe abuse during cycling in electrochemical cells, or upon heating to 500° C. The lithium ion intercalation process is considerably more complex than that for sodium ions; evidence for several ordering transitions is seen in the electrochemical potential spectroscopy experiments. These results are interpreted in terms of the unusual structure, and implications for future use of these materials in lithium batteries are discussed.

Introduction

Positive electrodes based on orthorhombic Na_xMnO_2 have recently been shown to undergo reversible ion intercalation processes in lithium and sodium polymer electrolyte cells[1]. Approximately 180 mAh/g can be utilized at moderately high voltages (3.7-2.5 V vs. Li, open circuit), allowing use of poly(ethylene oxide) or common ether or carbonate-based liquid electrolytes. The high capacities and voltages, ease of synthesis, low cost and low toxicity of this manganese oxide provide a compelling rationale for further development, but several questions must be answered before use in secondary lithium batteries can be realized. One question is that of the structural stability of the orthorhombic Na_xMnO_2 framework during lithium ion insertion and de-insertion processes. It is well-known that the spinel $LiMn_2O_4$ (or tetragonally distorted $Li_{1+x}Mn_2O_4$) structure is thermodynamically favored in oxides with Li:Mn ratios close to 1:2[2]. Numerous examples of rapid conversion to the spinel phase upon charge or discharge in lithium cells are known (e.g., γ-MnO_2[3], ramsdellite[4] and orthorhombic $LiMnO_2$[5]). Lithiated forms of orthorhombic Na_xMnO_2 are unusual in that they do not appear to undergo structural transformations under normal cell operating conditions, even at somewhat elevated temperatures (105° C). The limits of this meta-stability must, however, be determined, especially under conditions of cell abuse (overcharge, overdischarge and thermal events).

The details of the lithium ion insertion processes into this manganese oxide are clearly relevant to issues of rechargeability, rate capability and voltages of operating cells. The unusual tunnel structure of the manganese oxide framework is formed around sodium ions during synthesis of the $Na_{0.44}MnO_2$ precursor; these ions are then replaced by lithium during the subsequent "chimie douce" treatments (or *in situ* oxidation and reduction processes). Because lithium ions (0.68 Å) are smaller than sodium ions (0.97 Å), it is reasonable to believe that the sites in the tunnels are somewhat different for the latter than for the former. The slightly higher capacity of the orthorhombic Na_xMnO_2-based materials for lithium ions than for sodium also suggest differences in the insertion processes for the two ions. Electrochemical potential spectroscopy experiments on Na/Na_xMnO_2 cells[6] indicated that sodium ion intercalation is highly reversible over a wide composition range, and that several ordering transitions occur. Mixed alkali effects due to the presence of residual sodium ions, and the potential for formation of other phases complicate interpretation of lithium ion insertion processes in Li/Na_xMnO_2 cells. Herein, we present results on experiments designed to address issues of stability and intercalation processes in orthorhombic Na_xMnO_2-based materials for secondary lithium batteries.

Experimental

The precursor "$Na_{0.44}MnO_2$" was synthesized by heating together a sodium source and a manganese source (see table I) in the appropriate stoichiometric ratio for four to eight hours, in air, at 800° C. The resultant black powders were dry ball-milled for four hours and characterized by x-ray powder diffraction (Siemens D5000 diffractometer), and scanning electron microscopy. Alternatively, aqueous solutions of sodium nitrate, manganese nitrate and glycine were heated until spontaneous combustion occurred (glycine-nitrate combustion synthesis), and the reaction product calcined at 800° C for at least four hours. The very fine powders obtained by this method did not require further grinding. Samples were subjected to atomic absorption analysis for Na and Mn contents (University of California, Berkeley Microanalytical Laboratory) and surface area analysis (BET, Micromeritics, Norcross, GA). Typical elemental analyses and BET results for the different synthetic methods are summarized in Table 1.

Chemical oxidation of $Na_{0.44}MnO_2$ was carried out by stirring powders in a solution of aqueous hydrochloric acid (pH = 3) for twelve hours at room temperature. The product was filtered, washed well with de-ionized water and dried under vacuum at 80° C. Chemical exchanges were carried out by stirring together the precursor with a lithium salt, $LiCF_3SO_3$, (LiTf) or $LiN(CF_3SO_2)_2$ (LiTFSI, provided by 3M Corporation) in acetonitrile for up to twelve hours

(stoichiometric ratios or a two-fold excess of salt was used). Some samples were refluxed in acetonitrile with up to a ten-fold excess of salt for up to nine hours. Molten salt exchanges were carried out by heating $Na_{0.44}MnO_2$ with excess $LiNO_3$ in platinum crucibles above the melting point of the $LiNO_3$ (264° C) for twelve hours in air. Reduced (fully or partially lithiated) forms of Na_xMnO_2 were obtained by reaction with LiI or n-butyllithium. In the first case, $Na_{0.44}MnO_2$ was refluxed with a ten-fold excess of LiI in acetonitrile under argon for four hours. The product was washed well with acetonitrile under argon and vacuum dried. A sample of $Na_{0.44}MnO_2$ was reacted with a slight excess of n-butyllithium in hexane at -60° C under an inert atmosphere, in rigorously dried glassware. The reaction mixture was allowed to warm to ambient temperature gradually, and the contents were washed several times with dry hexane. The product was dried in vacuum. All of the "chimie douce" prepared samples were characterized by XRD and subjected to elemental analysis for Na, Li and Mn. The results are given in Table 2.

XRD patterns of samples derived from orthorhombic $Na_{0.44}MnO_2$ were indexed using the programs *Cell 5.0* by K. Dwight and *Powder Cell 1.7* by W. Kraus and G. Nolze. The structure shown in Figure 2 was constructed using the program *Atoms*.

Thermal decomposition limits of "chimie douce" materials were determined from XRD patterns of samples heated in alumina or platinum crucibles to the desired temperature for at least 12 hours. Thermogravimetric analyses were carried out on a Perkin-Elmer TGA-7 apparatus.

Electrodes and electrolytes for lithium/polymer cells were fabricated as described previously[1]. Lithium foil from Cyprus Foote Mineral Company was used for negative electrodes and cells were thermostatted in convection ovens controlled to ± 0.5° C for at least one hour prior to testing.

Cycling tests were performed on PAR 371 or 173 galvanostat/potentiostats controlled by software written in-house. Some galvanostatic experiments and the electrochemical potential spectroscopy experiments were carried out on a MacPile II from Bio-Logic, SA (Claix, France).

Results and Discussion

Synthesis and Structure of $Na_{0.44}MnO_2$

The precursor material, orthorhombic Na_xMnO_2, may be prepared with a nominal composition of x=0.44 via conventional solid state reactions or by solution methods. Formation of this phase is favored for reactant mixtures with Na/Mn molar ratios close to 0.44 between 800-1100° C in air, although other undesirable sodium manganese oxides[7] may form if the temperature or

stoichiometry deviate significantly. The composition of one sodium manganese oxide with the psilomelane structure, $Na_{0.4}MnO_2$, is close to that of orthorhombic $Na_{0.44}MnO_2$, but heating above 750° readily converts the former to the latter (some Mn_2O_3 is also produced). Synthesis of the precursor orthorhombic $Na_{0.44}MnO_2$ can, therefore, be accomplished readily and reproducibly via a number of different routes. Reactions between sodium carbonate and Mn_2O_3, sodium permanganate and Mn_2O_3, sodium carbonate and manganese carbonate, as well as glycine-nitrate combustion synthesis[8] with sodium nitrate and manganese nitrate were used successfully to produce the desired phase in this study. Very fine-grained powders are produced by the last method (1 in Table 1), obviating the need for a subsequent grinding step. However, scale-up of the combustion synthesis technique is not practical for this compound, and this route was eventually abandoned.

Elemental analyses for many of the products of these reactions indicated a slightly high manganese content for a formula of $Na_{0.44}MnO_2$. Additionally, peaks were evident in the XRD powder patterns that could be assigned to an Mn_2O_3 impurity. The amount varied with the synthetic procedure, and increased somewhat with increasing calcining times for some of the samples. Products made from $NaMnO_4$ and Mn_2O_3 tended to contain small amounts of Mn_2O_3 (estimated to be less than 5% of sample weight), and to show good crystallinity.

This synthetic procedure could also be reliably scaled up to 1 kg amounts. For these reasons, most of the work described herein was performed on samples produced by this reaction.

It is well-known that high surface areas and small grain sizes promote lithium diffusion in metal oxides[9]. Powders with surface areas of 6-8 M^2/g and a wide range of particle sizes in the micron range (judging from SEM images) are obtained after four hours of dry-ball milling $Na_{0.44}MnO_2$ produced by methods 2 and 3 in Table 1. The relatively high reaction temperature and long calcination times may be responsible for the fairly low surface areas. Shorter calcination times resulted in incomplete reaction. Sol-gel processing[10] may allow shorter reaction times and result in increased surface area, but has not yet been attempted.

The x-ray powder diffraction pattern of $Na_{0.44}MnO_2$ is shown in Figure 1. It is extremely complex, and, prior to this study, was indexed only by analogy to single crystal data on another compound, $Na_4Mn_4Ti_5O_{18}$[11]. Figure 1 also shows the calculated powder pattern for this compound obtained by Rietveld refinement. Differences in the observed and calculated patterns are attributable to the presence of Mn_2O_3 and preferred orientation of the sample. Figure 2 is a representation of the $Na_{0.44}MnO_2$ structure. Columns of edge-sharing MnO_5 square pyramids and sheets of edge-sharing MnO_6 octahedra two and three units in width extend parallel to the c-axis. These are connected by corner sharing to form two types of

tunnels. Each unit cell contains one large S-shaped tunnel containing four sodium sites, and two identical pentagonal tunnels, similar to those found in calcium ferrite, with a single sodium site. In as-prepared $Na_{0.44}MnO_2$, the sodium sites in the small tunnels are fully occupied, while the large-tunnel sites are half-occupied in an approximately random fashion.

"Chimie Douce" Reactions of $Na_{0.44}MnO_2$

Li/PEO/$Na_{0.44}MnO_2$ cells (PEO = poly(ethylene oxide)) have open circuit voltages of 3.2, exactly 0.3 V higher than those of Na/PEO/$Na_{0.44}MnO_2$ cells (Na^+/Na is -2.71 V vs. S. H. E. and Li^+/Li is -3.04). Approximately 0.24-0.31 Na^+/Mn may be oxidatively de-intercalated upon charging to 3.45 V in sodium cells or 3.77 V in lithium cells (i.e., the oxidative stability limits of PEO electrolytes). During charge, sodium eventually plates onto the lithium negative electrode, and may react with the electrolyte if it is not sufficiently stable towards sodium metal. (This does not, however, appear to be a problem with PEO, due to the kinetic stability of this electrolyte towards sodium[12]). For this reason, as well as to simplify studies of lithium intercalation processes, it is desirable to remove or replace the mobile sodium ions in $Na_{0.44}MnO_2$ prior to use in lithium cells. This may be achieved chemically under mild conditions ("chimie douce").

Air oxidation of $Na_{0.44}MnO_2$ occurs when powders are stirred in aqueous HCl (buffered to pH =3) for twelve hours at room temperature (this treatment also

removes the Mn_2O_3 impurity). Elemental analysis of the product indicates that the composition is $Na_{0.2}MnO_2$. $Li/Na_{0.2}MnO_2$ cells had open circuit voltages of 3.67-3.7 V and similar discharge characteristics to those of cells containing materials that were not subjected to the chemical oxidation. Some of the $Li/Na_{0.2}MnO_2$ cells, however, showed decreased capacity upon discharge and poor cyclability. $Na_{0.2}MnO_2$ produced by the aqueous acid treatment is difficult to dry, and the poor behavior may be due to occluded water, or the presence of protons (this is not readily detectable by elemental analysis, but evidence for occluded water is seen in TGA experiments).

Many manganese oxides are known to undergo ion exchange processes readily and are used for this purpose in some applications[13]. About half of the sodium ions are replaced with lithium when $Na_{0.44}MnO_2$ is stirred in solutions containing a slight excess of lithium salt for twelve hours at room temperature. More rigorous conditions (ten-fold excess of salt under reflux in acetonitrile) results in a higher degree of exchange, with 0.14 Na^+/Mn remaining after four hours and 0.11 Na^+/Mn after twelve. (It should be noted that partial exchange also occurs *in situ* if $Na_{0.44}MnO_2$ is used in lithium cells.) Complete replacement of sodium occurred only when $Na_{0.44}MnO_2$ was heated with excess $LiNO_3$ above the melting point of the latter (264° C) for twelve hours. The composition of the resultant product, $Li_{0.27}MnO_2$, indicated that both oxidation and exchange had taken place.

Lithium ion exchange capacities of 3.1 meq/g or 13.1 meq/cc can be calculated for $Na_{0.44}MnO_2$ based on the results of the "chimie douce" reactions.

$Li/Na_{0.44-x}Li_xMnO_2$ ($x \leq 0.3$) cells had open circuit voltages ranging from 3.2-3.39 V, with the more highly exchanged materials giving the upper values. The capacities of the initial charges tended to be lower for these cells as well, although the subsequent discharge capacities were not affected. Air oxidation of these samples may have taken place primarily during the electrode processing steps, as elemental analyses indicate that Mn contents are only slightly lower than expected for most samples. It has been pointed out that lithiated metal oxides with voltages lower than about 3.3 vs. Li are expected to be unstable in air with respect to Li_2CO_3 formation[14]. (Because the free energies of formation of Na_2CO_3, NaOH and Na_2O are lower than those of the corresponding lithium salts[15], $Na_{0.44}MnO_2$ is air-stable, even though it is in the partially reduced state). Susceptibility of lithiated materials to air oxidation is, therefore, a function not only of the degree of reduction, but also of the Li/Na ratio.

Reduction of Na_xMnO_2 may be carried out by reaction with LiI or n-butyllithium, under mild conditions. When $Na_{0.44}MnO_2$ is reacted with excess LiI, both reduction and exchange take place simultaneously, and it is possible to prepare partially lithiated samples. The practical composition limit is about $Na_{0.15}Li_{0.45}MnO_2$ using this method, and further reaction requires the use of a

stronger reducing agent, such as n-butyllithium. When $Na_{0.44}MnO_2$ was reacted with a slight excess of n-butyllithium, $Na_{0.38}Li_{0.36}MnO_2$ was formed, close to the composition predicted by the theoretical reversible reduction limit obtained in electrochemical experiments. Attempts to ion-exchange this material were only partly successful, and caused oxidation of the sample to occur instead. Thus, maximization of the Li/Na ratio in reduced samples requires that ion-exchange be carried out first, followed by careful reaction with n-butyllithium.

The expected potentials and practical composition limits of the chimie douce prepared samples are superimposed upon open circuit data obtained from electrochemical experiments (taken from reference 1) in Figure 3. In practice, cells containing the reduced samples gave potentials higher than expected, due to air oxidation during electrode preparation.

The XRD powder patterns of oxidized, exchanged and reduced samples are shown in Figure 4a-e, arranged in order of increasing average Mn oxidation state from bottom to top. The resemblance, in all four cases, to that of the parent compound is readily apparent, and there is no evidence for formation of other known phases in any of the patterns. For example, $Na_{0.2}MnO_2$ (Figure 4a) produced by the acid-catalyzed air oxidation is clearly not the same material as hollandite-type $Na_{0.2}MnO_2$ produced by solid state reactions. Neither is there evidence for formation of spinel $Li_{1+x}Mn_2O_4$ or other lithiated manganese oxides

in any of the lithiated samples. The progressive shifting of several peaks to lower 2θ values is consistent with an increase in the unit cell parameters due to reductive intercalation processes. The likelihood of some air oxidation of the n-butyllithium and LiI treated materials and the differing Li/Na ratios, however, complicate interpretation of these patterns.

Table 3 shows the unit cell parameters and volumes for manganese oxides derived from orthorhombic $Na_{0.44}MnO_2$, as a function of lithium content and oxidation state, based upon assignment to the space group *Pbam*. Both oxidation and replacement of sodium ions by lithium cause a decrease in the size of the unit cell; e.g., $Li_{0.27}MnO_2$ has a smaller unit cell than the more highly oxidized $Na_{0.2}MnO_2$. Similarly, the unit cell volume for $Na_{0.23}Li_{0.21}MnO_2$ is less than that of the unexchanged material. The unit cells of $Na_{0.44}MnO_2$ and $Na_{0.23}Li_{0.21}MnO_2$ are 4.3% and 2.6% larger, respectively, than that of $Na_{0.2}MnO_2$. It is not yet known whether similar changes are seen during electrochemical intercalation/de-intercalation processes, or exactly how the Li/Na ratio affects cell parameters. *In situ* XRD studies of Li/Na_xMnO_2 and Na/Na_xMnO_2 cells should shed light on these and other questions, but have not yet been performed.

The formula for partially exchanged samples, $Na_{0.23}Li_{0.21}MnO_2$, suggests that almost all the loosely bound sodium ions in the large tunnels (low voltage sites[6]) have been replaced, and that those in the small tunnels remain. Unfortunately,

attempts at Rietveld refinement of the XRD data for $Na_{0.23}Li_{0.21}MnO_2$ were unsuccessful at determining the distribution of lithium ions in this compound. The results of both the "chimie douce" and molten salt exchanges indicate that removal of sodium from the small tunnels is possible, but is more difficult than removal from the large tunnels.

Stability Studies

Orthorhombic Na_xMnO_2 that contains lithium (or with x different than 0.44), is expected to be thermodynamically unstable with respect to formation of other phases such as $Li_{1+x}Mn_2O_4$ spinel. A degree of meta-stability for this compound is implied from the above results and the cycling experiments in lithium cells[1]. If the kinetic barrier is sufficiently high, phase conversions predicted from thermodynamic considerations will not occur under normal cell operating conditions. For example, the non-stoichiometric oxide, P2 Na_xCoO_2, may be cycled in sodium cells over a composition range of x=0.3-0.9 without disruption of the structure[16], although several other phases that fall within this composition range exist. In practice, conversion does not occur except at extremely high temperatures.

The limits to the thermal meta-stability of lithium-containing orthorhombic Na_xMnO_2s and $Na_{0.2}MnO_2$s were estimated by heating samples to given temperatures, in air, for twelve hours, cooling them slowly, and obtaining XRD

patterns. Lithiated samples produced by chemical exchange or reduction were somewhat more prone to air oxidation as the temperature was increased (i.e., there was a systematic shifting of several peaks to higher 2θ), but no evidence for formation of other manganese oxide phases was seen below 500° C. After heating to 500° C for twelve hours, numerous peaks in the XRD pattern shifted to lower 2θ, and new peaks attributable to the tetragonally distorted spinel, $Li_{1+x}Mn_2O_4$, were observed. This is consistent with decomposition of lithiated Na_xMnO_2s to $Na_{0.44}MnO_2$ and $Li_{1+x}Mn_2O_4$; the relative amount of each produced being dependent upon the Li/Na ratio of the starting material.

Similar experiments on chemically produced $Na_{0.2}MnO_2$ indicated that decomposition to $Na_{0.44}MnO_2$ and Mn_2O_3 occurs only above 400° C, in air. (No evidence for $Na_{0.2}MnO_2$ with the hollandite structure was seen). A representative thermogravimetric analysis trace for this reaction (under nitrogen) is shown in Figure 5. The weight loss below 200° C is approximately 0.5%, even for this well-dried sample. (This amount varied considerably with drying procedure, with some samples exhibiting much higher losses attributable to occluded water). The onset of the decomposition reaction is observed slightly below 400° C in nitrogen and results in a further decrease of 4.65% (Δ%). Loss of oxygen, according to reaction 1, should result in a total weight change of 4.75%.

$$2.2Na_{0.2}MnO_2 \longrightarrow Na_{0.44}MnO_2 + 0.6Mn_2O_3 + 0.3O_2 \uparrow \quad (1)$$

Clearly, orthorhombic Na_xMnO_2s resemble the sodium cobalt oxide example given above in that considerable thermal energy is required for the bond breaking and re-arrangement necessary to convert to other phases. Thus, the observed meta-stability during normal cycling in lithium cells is perhaps not surprising.

Figure 6 shows capacity as a function of discharge number for a polymer electrolyte cell that failed catastrophically after two months of operation at 105° C. It was cycled between various voltage limits, at current densities of 0.05 mA/cm^2 (charge) and, eventually, 0.2 mA/cm^2 (discharge) except as indicated in the figure caption. (The apparent initial decrease in the capacity is due to changes in the discharge current during the initial cycles). Coulombic inefficiencies of a few percent were observed during the first fifty charges, which may have been caused by electrolyte oxidation due to the high upper voltage limit. After fifty cycles, however, voltage instability upon charge was seen, attributable to dendrite formation. Very long over-charges (sometimes as much as 300% of the capacity obtained during the previous discharge) were required on some cycles to compensate for the soft shorting. Dendrite formation became progressively worse, and the discharges immediately after particularly severe episodes tended to show low capacity, but recovered to normal thereafter. After eighty-four cycles, the capacity dropped precipitously and the cell could no longer be charged above

3.1 V. An XRD powder diffraction pattern obtained from the cycled cathode indicated that conversion to a poorly crystalline form of $Li_{1+x}Mn_2O_4$ had occurred. This was the only instance in this study that conversion of the active material to spinel was observed in electrochemical cells. It is probable that a cumulative over-reduction of orthorhombic Na_xMnO_2 occurred during the repeated episodes of soft shorting, eventually resulting in phase conversion. Single instances of moderate over-discharge (e.g., to voltages as low as 1.5) does not appear to cause substantial damage to the Na_xMnO_2 structure, while charging to high voltages appears only to damage the electrolyte. No evidence for spinel formation was seen in Li/PEO/Na_xMnO_2 cells heated to 95-105°C and held in discharged or partially discharged states for up to three months (the longest test period for this study). The cathode material in cells cycled normally over a similar length of time also remained intact.

Characterization of Electrochemical Lithium Insertion Processes

Information on sodium intercalation into orthorhombic Na_xMnO_2 serves as a useful guideline for the analogous, but more complex, lithium insertion process. It has been found experimentally that the composition of Na_xMnO_2 can be varied over the approximate range x=0.15-0.7 during charge/discharge in sodium/polymer cells[1]. Complete filling of all sites shown in Figure 2 leads to a formula of $Na_{0.66}MnO_2$; thus the limit to reversible reductive intercalation is

structurally determined. Complete removal of sodium ions from only the large tunnels should lead to a composition of $Na_{0.22}MnO_2$; the formulas of the electrochemically and chemically oxidized materials ($Na_{0.2}MnO_2$) indicate that removal of at least some ions from the small tunnels is possible as well. The upper composition limit is determined primarily by the oxidative stability of the PEO electrolyte, not by structural considerations; preliminary results indicate that all of the sodium and lithium ions may be removed electrochemically from orthorhombic Na_xMnO_2 without inducing structural damage.

The higher capacity of Na_xMnO_2 for lithium ions (to a total alkali metal ion content as high as 0.8 M^+/Mn) implies that this insertion process is somewhat different than that for sodium ions. Lithium ions (0.68 Å) are smaller than sodium (0.97 Å), allowing more of the former to be accommodated in the large S-shaped tunnels, although the sites are probably different from those shown in Figure 2 for sodium ions.

The complexity of the XRD patterns for orthorhombic Na_xMnO_2 makes interpretation difficult. For this reason, electrochemical potential spectroscopy (ECPS)[17] was used to obtain information on ion insertion processes. In this technique, the cell potential is stepped in small increments very slowly, and current or charge is measured as a function of time. Kinetic data may be obtained from the current response during each potential step, while differential capacity

plots may be used to observe phase or ordering transition phenomena. Integration of the latter also allows quasi-OCV data to be obtained.

The dQ/dV plots taken from ECPS experiments on typical Na/PEO/Na_xMnO_2 and Li/PEO/Na_xMnO_2 cells are shown in Figures 7a and b. A comparison between the two is highly instructive. Both exhibit excellent reversibility and pseudo-capacitative behavior typical of a single phase system (i.e., significant capacity is seen throughout the entire voltage range). The extremely sharp peak at 3.22 V in Figure 7a occurs at x=0.22 in Na_xMnO_2 and is associated with ordering or preferential filling of ions in the small tunnels[6]. An analogous, but broader, peak is exhibited at 3.39 V for the lithium case, also at x=0.22 in M_xMnO_2 (where M=Li + Na). A voltage of 3.52 for this ordering transition in lithium cells is predicted if only the difference in reduction potentials for Li^+ and Na^+ is taken into account. The chemical potential for lithium ions is, therefore, not the same as that for sodium ions at this composition, implying an altered environment for the former. The smaller lithium ions may be positioned off-center in the small tunnels, and/or changes in the unit cell dimensions may be responsible for these differences.

A broad feature centered at about 3.05 V in the differential capacity plot for the Na/PEO/Na_xMnO_2 cell is associated with preferential filling of the first of four sites in the large tunnels (x=0.33 in Na_xMnO_2). A more distinct peak appears at

3.1 V in the Li/PEO/Na_xMnO_2 cell for a composition of $M_{0.34}MnO_2$. Again, the differences in shape and position of this peak imply different sites for lithium than for sodium in the large tunnels.

The shapes, relative magnitudes and positions of the peaks in the Li/PEO/Na_xMnO_2 differential capacity plots are affected in a complex manner by the degree of exchange in the cathode material. For example, the peak at about 3.1 V is much sharper and the high voltage peak is shifted downward for more highly exchanged samples. Li/PEO/$Na_{0.23}Li_{0.21}MnO_2$ cells exhibit a peak at 3.07 V upon which is superimposed an additional small peak on the first cycle; the main peak then shifts slightly after several cycles and the small peak disappears. These changes are not seen in the samples that initially had a higher Li/Na ratio. This is indirect evidence of *in situ* exchange occurring, and suggests that some sodium ions are located in the large tunnels for $Na_{0.23}Li_{0.21}MnO_2$ samples. Residual sodium ions in the orthorhombic Na_xMnO_2 structure apparently affect the chemical potentials (positions) of the lithium ions in subtle ways not readily detected in galvanostatic experiments. ECPS may therefore be used as a "fingerprint" technique to determine the distribution of sodium and lithium ions in this very complex system.

The Na_xMnO_2 cathode active material is fully intercalated by 2.2 V in sodium cells, under the near-equilibrium conditions of the ECPS experiment. Two

additional sets of peaks corresponding to filling of 3/4 of the sites (x=0.55), and all of the sites (x=0.66) in the large tunnels are observed below 2.9 V in the dQ/dV data. In lithium cells, only 65% utilization of the positive electrode is achieved by 2.5 V. For the cell in Figure 7b, the composition at this point is $Na_{0.14}Li_{0.38}MnO_2$, and there are approximately 3 Li^+/Mn located in the large tunnels.

Additional intercalation of lithium into orthorhombic Na_xMnO_2 under these conditions requires stepping the potential below 2.5 V. Figure 8 shows ECPS data for a Li/PEO/Na_xMnO_2 cell between 2.1 and 3.6 V. A large peak below 2.45 V is seen during cell discharge, but not upon cell charge. The current response to the potential step during cell discharge is strikingly different below 2.45 V as well. In the reversible region above 2.5 V, the current decays rapidly, following the expected $t^{-1/2}$ behavior for rate-determining diffusional processes[18]. Below 2.45 V, it rapidly drops to a fraction of the initial value, but thereafter decreases only gradually (Figure 9). After two hours, there is still significant current, and its magnitude increases linearly as the voltage is stepped further. This, as well as the asymmetry of the dQ/dV plot in this region, is characteristic of a rate-limiting first order phase transition. During the transformation, the faradaic component of the current remains nearly constant with time, but varies linearly with the polarization (difference between the applied voltage and the OCV of the two phase region)[19].

This allows an open circuit voltage of 2.42 to be calculated for this two phase region in lithiated Na_xMnO_2.

The recharge and subsequent (second) full discharge of the cell is also shown in Figure 8. A new peak appears at about 2.65 V during charge, but not during the second discharge, and a broad quasi-reversible peak appears at about 3.15 V. No manganese-containing phases except Mn_2O_3 and orthorhombic Na_xMnO_2 were detected in the XRD powder pattern obtained on the cathode from this deeply discharged cell. It appeared, however, that the amount of Mn_2O_3 had increased somewhat as a result of this treatment. All cells discharged to open circuit voltages below 2.5 exhibited a peak at about 2.65 V in the ECPS upon charge, but not necessarily the coalescence of the two reversible peaks above 3 V. This feature is apparently associated with completion of the phase transition below 2.5 V (return of the current response to normal $t^{-1/2}$ behavior). This requires long periods of time below 2.5 V; e.g., 160 hours for the cell in Figure 8 at 85° C.

Interestingly, a reversible peak at about 3.15 V, as well as peaks at 3.33 and 3.08 V, are seen in the dQ/dV data of lithium cells containing Li_xMnO_2 produced by molten salt exchange (Figure 10a), even prior to discharge below 2.5 V. Figure 10b shows the second discharge to 2.1 V and subsequent charge of the same cell. The open circuit voltage of the two phase region is calculated to be 2.5 V, and the phase transformation is completed more rapidly (80 hours) than for the sodium-

containing manganese oxide cathodes. It also appears to take place in two distinct steps. An increase in the relative amount of Mn_2O_3 was detected in the XRD powder pattern of the cycled cathode, and the peaks attributable to Li_xMnO_2 obtained from the orthorhombic $Na_{0.44}MnO_2$ had broadened considerably. No spinel phases were detected.

The results of the ECPS experiments in Figures 8 and 10b are consistent with strong ordering of lithium ions upon reduction of cathode active material below 2.5 V, followed by a slow decomposition reaction resulting in an increase in the amount of electrochemically inactive Mn_2O_3 (e.g., a displacement reaction). The presence of sodium ions in the structure apparently retards these processes to some degree. Furthermore, an electroactive material is produced that is either undetectable in the XRD experiments (amorphous) or is very closely related to the original orthorhombic Na_xMnO_2 structure. This could be, for example, an ordered or a defect phase. Some of the same material is apparently produced under the conditions of the molten salt exchange. Surprisingly, there is no immediate loss of capacity associated with the deep discharge, although the depression of the average cell voltage implies a loss of energy density.

It is not possible to calculate lithium ion diffusion coefficients for orthorhombic Na_xMnO_2 below 2.5 V in Li/Na_xMnO_2 cells because of the complications from the slow phase transformation. Above 2.5 V, diffusion

coefficients of 10^{-11}-10^{-12} cm^2/sec at 85° C are estimated from the potentiostatic intermittent titration, assuming an average particle radius of 1 μm. Because measurements were obtained on composite electrodes, in which the contact area, S, between the cathode and electrolyte is not well-known, there is a great deal of uncertainty in these numbers. Nevertheless, a comparison of diffusion coefficients as a function of state of charge of Na_xMnO_2 is valid. Interestingly, there does not seem to be a significant difference in rates of lithium ion diffusion into the small and large tunnels in the reversible region. However, a moderate decrease in rate is seen near the two reversible ordering transitions, as expected.

The effect of the slow kinetics of the low voltage phase transformation is reflected in the asymmetry of galvanostatic discharge and charge profiles of Li/PEO/Na_xMnO_2 cells (Figure 11). Discharges exhibit a pronounced inflection not seen in the subsequent charges, the position of which depends upon current density and other factors. For the example in Figure 11, this occurs somewhat earlier than the 117 mAh/g predicted from the ECPS experiment. Under typical operating conditions, far from equilibrium, some of the cathode material may be unevenly reduced due to wide grain size distributions (as is the case here) or cell geometry effects. Nevertheless, all of the capacity can be recovered on the subsequent charge, and the cell can be cycled.

If cells are open-circuited when discharged past the inflection point, but before the cathode is totally utilized, the voltage rises quickly as much as 0.7 V. The operating voltage drops again when the current is resumed, even after long rest periods. The observed decrease in voltage is, therefore, attributable mainly to the slow kinetics of the phase transformation in Na_xMnO_2 and not to mass transfer or polarization effects.

The discharge characteristics of Li/Na_xMnO_2 cells depend upon the starting composition of the manganese oxide cathode active material. A higher initial Li/Na ratio results in greater discharge capacities between operating voltages of 1.8 and 3.77. This is shown in Figure 12, for two $Li/PEO/Na_xMnO_2$ cells at four hour rates. $Na_{0.14}Li_{0.3}MnO_2$ may be discharged more deeply than $Na_{0.23}Li_{0.21}MnO_2$, even though the current density used and cathode capacity (thickness) is somewhat greater. The position of the inflection in the discharge profile also occurs somewhat later for the more highly exchanged sample. The completely exchanged Li_xMnO_2 manifested a slightly lower discharge capacity than any of the sodium-containing materials; this is probably attributable to the earlier onset of the displacement reaction. For optimum performance, it is, therefore, desirable to keep some sodium in the orthorhombic Na_xMnO_2 cathode material to stabilize the structure. For $Na_{0.14}Li_{0.3}MnO_2$, enough sodium is present to optimize the discharge capacity, but *in situ* ion exchange does not occur, nor

does the residual sodium participate in electrochemical processes under these operating conditions. Because the sodium ions are most likely located in the small tunnels, no interference with lithium intercalation processes into the large tunnels is expected to occur.

Operation of cells at low voltages is undesirable both because of the eventual destruction of the cathode active material and because the drop in power output is too great for many applications. Optimization of surface areas and particle size distributions in orthorhombic Na_xMnO_2 should maximize the discharge capacity of cells between 3.77 and 2.5 V, at least to the theoretical limit of 117 mAh/g. However, under the conditions used in this study, 0.2 cations/Mn are typically left in the small tunnels of the orthorhombic Na_xMnO_2 structure at the end of charge. Preliminary results indicate that these cations may be removed electrochemically above 3.7 V without damaging the structure, provided a sufficiently stable electrolyte is used. This additional capacity completely compensates for that presently obtained below the inflection point in the discharge curves. The 60 mAh/g accessible at the low voltages need not be utilized under normal operating conditions, but could serve instead as a measure of over-discharge protection.

Alternatively, stabilization of the structure could be achieved by doping it with other metals; preferably those that are low cost and environmentally benign, like titanium. The existence of the structural analog, $Na_4Mn_4Ti_5O_{18}$, indicates that

solid solutions containing up to 60 atom % titanium may be prepared. Further work in this laboratory will be directed towards studying titanium-doped orthorhombic Na_xMnO_2s with the goal of improving the reversible capacity in lithium polymer cells and increasing the cycle life.

Conclusions

Lithiated orthorhombic Na_xMnO_2 is a promising material for use in rechargeable lithium/polymer batteries. It exhibits a high reversible capacity for lithium ion intercalation processes at voltages compatible with PEO electrolytes, and does not convert to the spinel phase under normal cell cycling conditions. Manganese oxides are, in general, notorious for phase instability, so the observed meta-stability of the orthorhombic Na_xMnO_2 is an especially striking and desirable feature. Electrochemical potential spectroscopy experiments were used to study the lithium ion insertion processes into Na_xMnO_2, which are considerably more complex than the analogous sodium insertion processes. Two reversible ordering transitions and a kinetically slow phase transformation are observed in the differential capacity plots. Suggestions for further improving the discharge characteristics of orthorhombic Na_xMnO_2 are given and include increasing the surface area, narrowing the particle size distribution and doping with titanium.

Acknowledgment: This work was supported by the United States Advanced Battery Consortium (USABC) under a cooperative research and development agreement with the Lawrence Berkeley Laboratory. The USABC is a partnership of Chrysler, Ford and General Motors, with technical and financial participation of the Electric Power Research Institute (EPRI)/utilities and the United States Department of Energy. The program manager for this work is Dr. Robert Swaroop.

References

[1] M. M. Doeff, M. Y. Peng, Y. Ma and L. C. De Jonghe, *J. Electrochem. Soc.*, **141**, L145 (1994).

[2] M. M. Thackeray, A. de Kock, M. H. Roussow, D. Liles, R. Bittihn and D. Hoge, *J. Electrochem. Soc.*, **139**, 363 (1992).

[3] R. J. Neat and R. J. Powell *United States Patent 5,030,523* (1991).

[4] M. M. Thackeray, M. H. Roussow, R. J. Gummow, D. C. Liles, K. Pearce, A. De Kock, W. I. F. David and S. Hull, *Electrochim. Acta,* **38**, 1259 (1993).

[5] R. J. Gummow, D. C. Liles and M. M. Thackeray, *Mat. Res. Bull.*, **28**, 1249 (1993).

[6] M. M. Doeff, L. Ding and L. C. De Jonghe, *Proc. Mat. Res. Soc.*, in press.

[7] J.-P. Parant, R. Olazcuaga, M. DeValette, C. Fouassier, and P. Hagenmuller, *J. Solid State Chem.*, **3**, 1 (1971).

[8] L. R. Pederson, G. D. Maupin, W. J. Weber, D. J. McReady, and R. W. Stephens, *Mat. Lett.*, **10**, 437 (1991).

[9] a) P. Barboux, J. M. Tarascon and F. K Shokoohi, *J. Sol. State Chem.*, **94**, 185 (1991). b) A. de Kock, M. H. Roussow, L. A. de Picciotto, M. M. Thackeray, W. I. F. David, and R. M. Ibberson, *Mater. Res. Bull.*, **25**, 657 (1990).

[10] a) A. Rousset, F. Chassagneux and J. Paris, *J. Mater. Sci.*, **21**, 3111 (1986). b) H. Huang and P. G. Bruce, *J. Electrochem. Soc.*, **141**, L76 (1994).

[11] W. G. Mumme, *Acta Cryst.*, **B24**, 1114 (1968).

[12] a) K. West, B. Zachau-Christiansen, T. Jacobsen, E. Hiort-Lorenzen and S. Skaarup, *Brit. Polymer J.*, **20**, 243 (1988). b) Y. Ma, M. M. Doeff, S. J. Visco and L. C. De Jonghe, *J. Electrochem. Soc.*, **140**, 2726 (1993).

[13] a) M. Tsuji and S. Komarneni, *J. Mater. Res.*, **8**, 611 (1993) and references therein. b) X.-M. Shen and A. Clearfield, *J. Solid State Chem.*, **64**, 270 (1986).

[14] W. Li, W. R. McKinnon and J. R. Dahn, *J. Electrochem. Soc.*, **141**, 2310 (1994).

[15] *Handbook of Chemistry and Physics,* R. C. Weast, editor, 68th edition, CRC Press Inc., Boca Raton, FL (1987-1988).

[16] a) C. Delmas, J.-J. Braconnier, C. Fouassier and P. Hagenmuller, *Sol. State Ionics,* **3/4**, 165 (1981). b) L. W. Shacklette, T. R. Jow and L. Townsend, *J. Electrochem. Soc.*, **135**, 2669 (1988).

[17] A. H. Thompson, *J. Electrochem. Soc.*, **126**, 608 (1979).

[18] C. J. Wen, B. A. Boukamp, and R. A. Huggins, *J. Electrochem. Soc.*, **126**, 2258 (1979).

[19] Y. Chabrè and J. Pannetier, *Prog. Solid St. Chem.*, **23**, 1 (1995).

Table 1. Elemental Analyses and Surface Areas of Representative Samples of Orthorhombic Na_xMnO_2 Precursors

Synthesis method	**Sodium Source**	**Manganese Source**	**Conditions**	**% Na[a]**	**% Mn[b]**	**Surface Area, M^2/g**
1	$NaNO_3$	$Mn(NO_3)_2$	glycine-nitrate combustion	10.3	56.5	N/A
2	$NaMnO_4$	Mn_2O_3	8 hours at 800° C, in air	10.5	57.6	6[c]
3	Na_2CO_3	Mn_2O_3	8 hours at 800° C in air	9.8	56.9	8[c]
4	Na_2CO_3	Mn_2O_3	4 hours at 800° C in air	10.4	54.6	N/A

a) expected Na content for $Na_{0.44}MnO_2$: 10.42%

b) expected Mn content for $Na_{0.44}MnO_2$: 56.62%

c) after four hours dry ball-milling.

Table 2. Elemental Analysis on Some "Chimie Douce" Prepared Samples

Precursor synthesis (from Table 1) and subsequent treatment	% Na	% Li	% Mn	Formula
1, followed by aqueous acid oxidation[a]	5.0	—	60.2	$Na_{0.2}MnO_2$[b]
2, stirred with 2-fold excess LiTf in acetonitrile[a]	5.53	1.50	59.40	$Na_{0.23}Li_{0.21}MnO_2$[c]
2, refluxed with 10-fold excess LiI in acetonitrile	3.82	3.31	58.10	$Na_{0.15}Li_{0.43}MnO_2$[d]
2, reduction with n-butyllithium	9.14%	2.63	54.90	$Na_{0.38}Li_{0.36}MnO_2$[e]

a) room temperature

b) expected for $Na_{0.2}MnO_2$: Na-5.02%, Mn-60.03%

c) expected for $Na_{0.23}Li_{0.21}MnO_2$: Na-5.65%, Li-1.27%, Mn-58.9%

d) expected for $Na_{0.15}Li_{0.43}MnO_2$: Na-3.7%, Li-3.19%, Mn-58.8%. The slightly low Mn content may be a result of air oxidation.

e) expected for $Na_{0.38}Li_{0.36}MnO_2$: Na-8.9%, Li-2.55%, Mn-55.95%. The slightly low Mn content may be a result of air oxidation.

Table 3. Unit cell parameters and volumes for manganese oxides derived from $Na_{0.44}MnO_2$ (space group *Pbam*).

Formula	Preparation Method	Cell Parameters, Å			Cell Volume, $Å^3$
		a	b	c	
$Na_{0.44}MnO_2$	2 (Table 1)	9.10	26.34	2.82	676
$Na_{0.2}MnO_2$	1, followed by acid treatment	9.045	25.32	2.83	648
$Na_{0.23}Li_{0.21}MnO_2$	2, followed by exchange	9.145	25.78	2.82	665
$Li_{0.27}MnO_2$	2, followed by exchange with molten $LiNO_3$	8.198	24.09	2.83	607

Figure Captions

Figure 1. (Lower trace) X-ray powder diffraction pattern of $Na_{0.44}MnO_2$ produced by method 2 in Table 1. The most prominent peak attributable to small amounts of Mn_2O_3 in the sample is marked with an asterisk. (Upper trace) calculated x-ray powder diffraction pattern of $Na_{0.44}MnO_2$ obtained by Rietveld refinement. The program *Powder Cell 1.7* was used to produce the pattern.

Figure 2. The proposed structure of $Na_{0.44}MnO_2$. Sodium ions or potential sites for sodium ions are represented by spheres.

Figure 3. Expected potentials and composition range limits for "chimie douce" prepared samples of Na_xMnO_2 superimposed upon open circuit data of $Li/Na_{0.2}MnO_2$ cells (taken from reference 1).

Figure 4. X-ray powder diffraction patterns of samples prepared by "chimie douce" methods arranged in order of oxidation state of the Mn. a) $Na_{0.2}MnO_2$ made by an acid-catalyzed air oxidation of $Na_{0.44}MnO_2$. b) $Li_{0.27}MnO_2$ prepared by molten salt exchange. c) $Na_{0.23}Li_{0.21}MnO_2$ prepared by a solution exchange reaction. d) $Na_{0.15}Li_{0.43}MnO_2$ prepared by reaction with LiI in solution. e) $Na_{0.38}Li_{0.36}MnO_2$ prepared by reaction with n-BuLi in solution.

Figure 5. Thermogravimetric analysis of the decomposition reaction of $Na_{0.2}MnO_2$ under nitrogen. The sample had been dried at 350° C in air for twelve hours, prior to the experiment. Scan rate 2° C/min.

Figure 6. Capacity as a function of discharge number for a $Li/PEO_8LiTFSI/Na_{0.23}Li_{0.21}MnO_2$ cell (0.81 mAh/cm^2) operated at 105° C. The cell was cycled between the voltage limits indicated on the graph. The capacity for the first discharge (50 $\mu A/cm^2$) was 174 mAh/g. The current density for the next six discharges was 0.1 mA/cm^2, and for all subsequent discharges was 0.2 mA/cm^2. All charges were at 50 $\mu A/cm^2$.

Figure 7. Differential capacity plots obtained from ECPS experiments on a) a $Na/PEO_{20}NaTf/Na_xMnO_2$ cell (taken from reference 6) and a b) $Li/PEO_8LiTFSI/Na_xMnO_2$ cell operated at 85° C (starting composition $Na_{0.14}Li_{0.3}MnO_2$). The potential was stepped 5 mV every 2 hrs between 2.215 and 3.35 V for the sodium cell and 10 mV every 4 hrs between 2.5 and 3.6 V for the lithium cell. The upper traces on each plot represent cell charges, and the lower traces cell discharges.

Figure 8. A differential capacity plot obtained from an ECPS experiment on a $Li/PEO_8LiTFSI/Na_xMnO_2$ cell operated at 85° C. The starting composition was $Na_{0.14}Li_{0.30}MnO_2$. The potential was stepped 10 mV every four hours from 3.6 to 2.1 V (♦), then back to 3.6 V (x) and finally to 2.5 V (x). The upper trace represents cell charge, and the lower the cell discharges.

Figure 9. Current response of a $Li/PEO_8LiTFSI/Na_xMnO_2$ cell to a -10 mV potential step from 2.60 to 2.59 V (●) and 2.37 to 2.36 V (◊).

Figure 10. a) A differential capacity plot obtained from an ECPS experiment on a $Li/PEO_8LiTFSI/Na_xMnO_2$ cell operated at 85° C. The potential was stepped 10 mV every four hours between 3.6 and 2.5 V. The upper trace represents cell charge and the lower cell discharge. b) An ECPS trace of the second discharge and charge of the cell in a. The potential was stepped 10 mV every four hours between 3.6 and 2.1 V. The lower trace represents the second discharge of the cell, and the upper trace the subsequent re-charge.

Figure 11. The first discharge and subsequent charge of a $Li/PEO_8LiTFSI/Na_xMnO_2$ (0.46 mAh/cm^2) cell operated at 85° C. The starting composition was $Na_{0.14}Li_{0.3}MnO_2$ and the cell was partially charged prior to the first discharge. The current density was 0.115 mA/cm^2 during discharge, and 0.05 mA/cm^2 during charge. There was a one hour open circuit period between half cycles, and voltage limits of 3.77 and 1.8 V were used.

Figure 12. First discharges of two Li/PEO_8LiTFSI/Na_xMnO_2 cells operated at 85° C. A lower voltage cutoff of 1.8 was used. Both cells were partially charged to 3.77 V and allowed to remain on open circuit for one hour prior to discharge. a) Starting composition was $Na_{0.14}Li_{0.3}MnO_2$, capacity was 0.46 mAh/cm^2, and the current density was 0.115 mA/cm^2. b) Starting composition was $Na_{0.23}Li_{0.21}MnO_2$, capacity was 0.4 mAh/cm^2, and the current density was 0.1 mA/cm^2. The spikes in this voltage profile are due to periodic current interrupts lasting 1 minute.

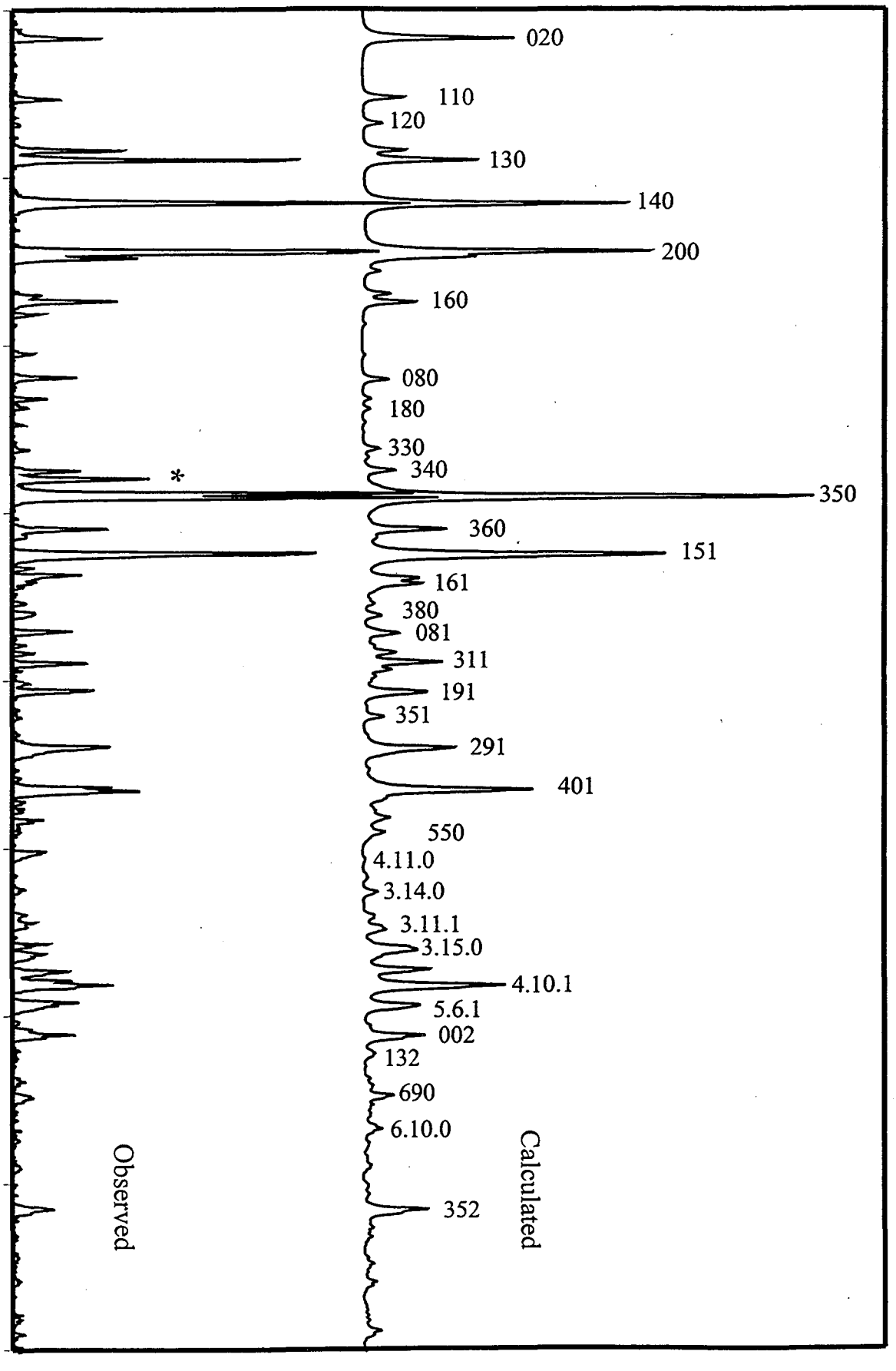
Counts
5
15
25
35
45
55
65
75
85
2θ
020
110
120
130
140
200
160
080
180
330
340
*
350
360
151
161
380
081
311
191
351
291
401
550
4.11.0
3.14.0
3.11.1
3.15.0
4.10.1
5.6.1
002
132
690
6.10.0
352
Observed
Calculated

Figure 1

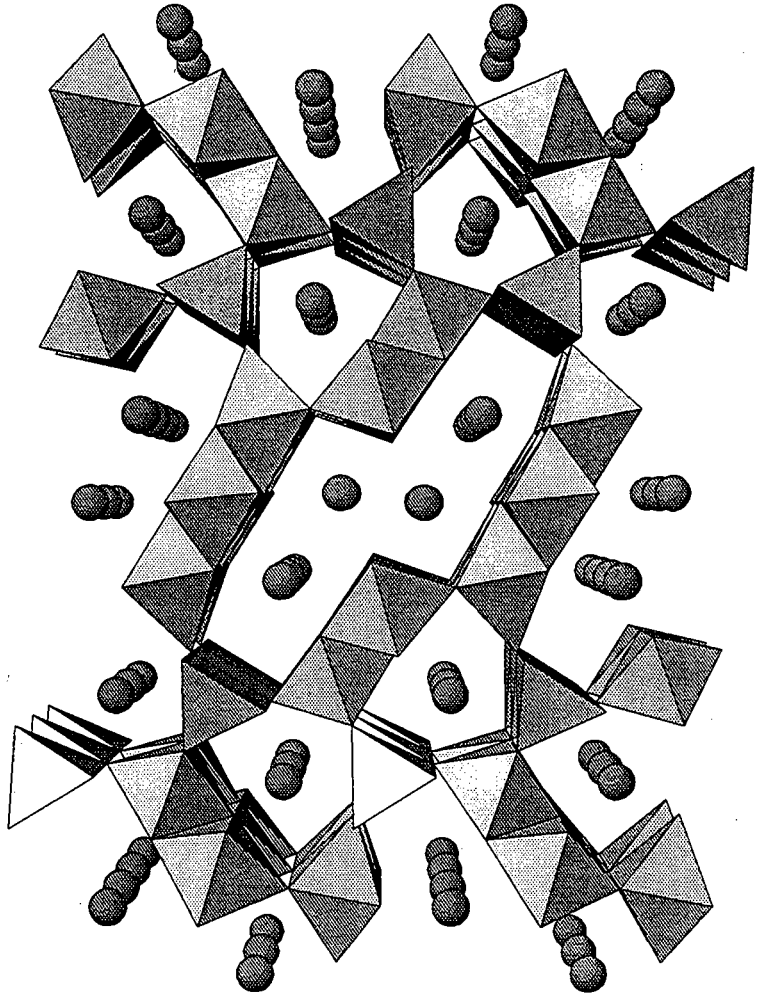

Figure 2

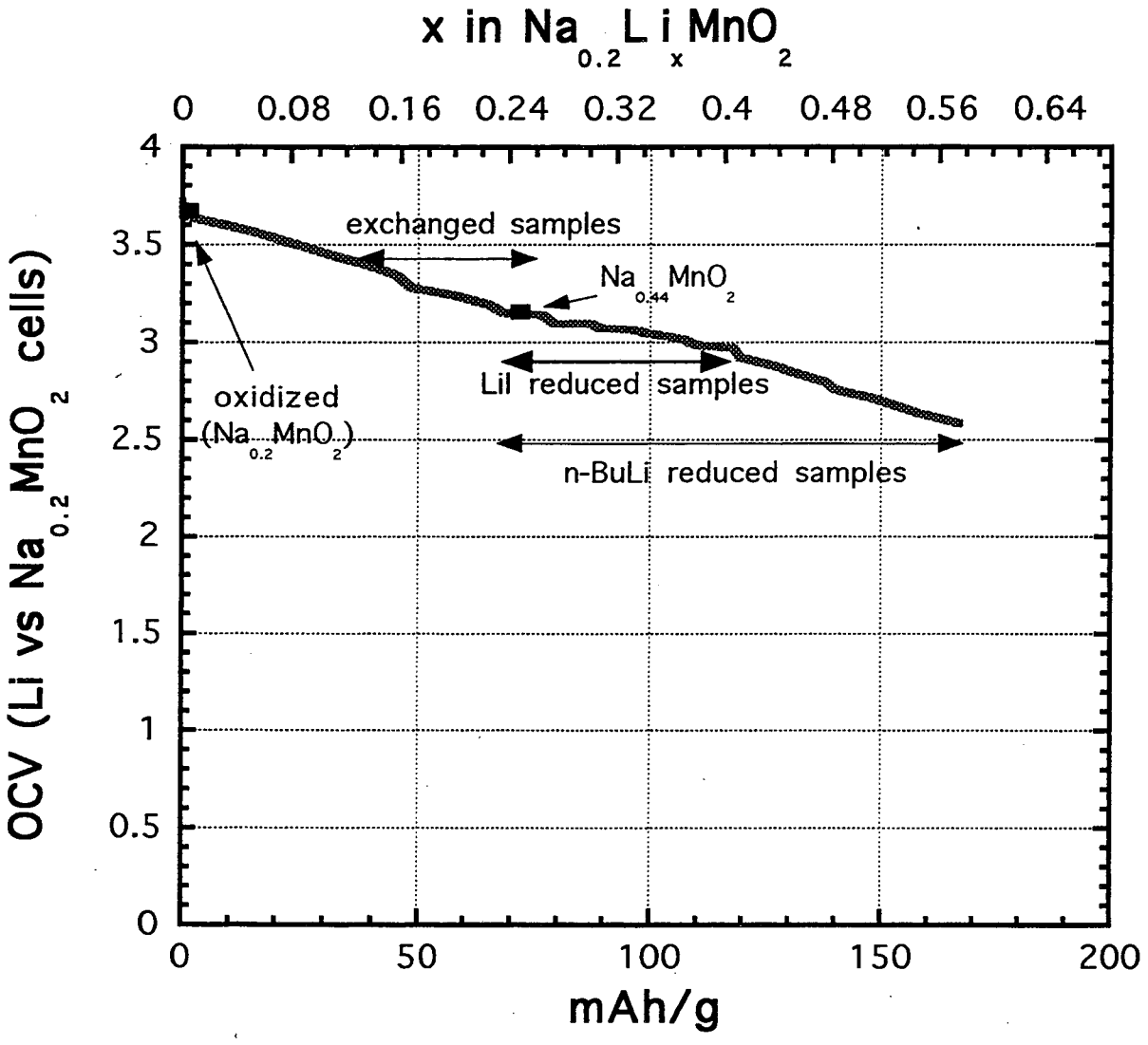
x in Na0.2LixMnO2
0
0.08
0.16
0.24
0.32
0.4
0.48
0.56
0.64
OCV (Li vs Na0.2MnO2 cells)
4
3.5
3
2.5
2
1.5
1
0.5
0
exchanged samples
Na0.44MnO2
LiI reduced samples
oxidized
(Na0.2MnO2)
n-BuLi reduced samples
0
50
100
150
200
mAh/g

Figure 3

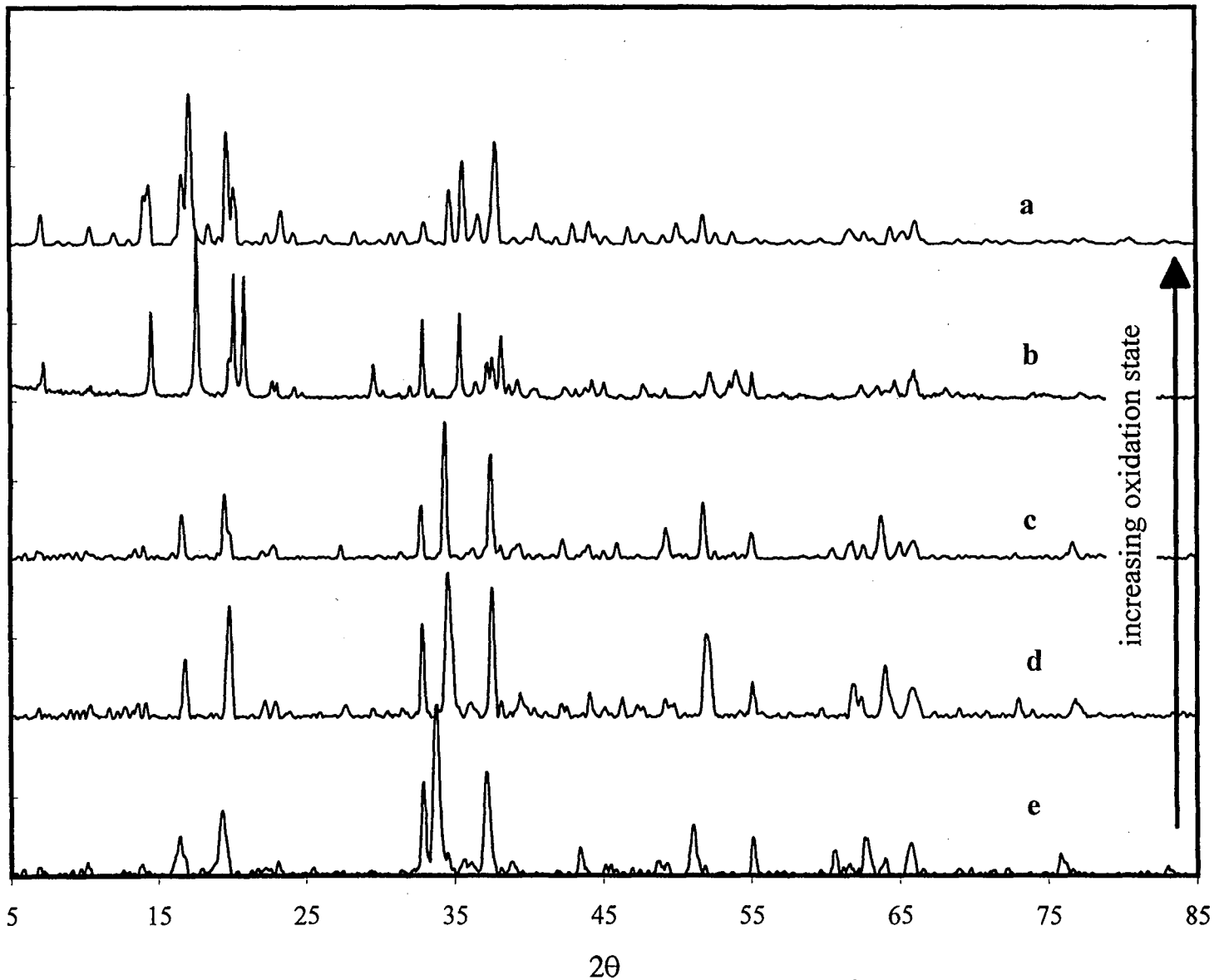
Counts
a
b
c
d
e
increasing oxidation state
5
15
25
35
45
55
65
75
85
2θ

Figure 4

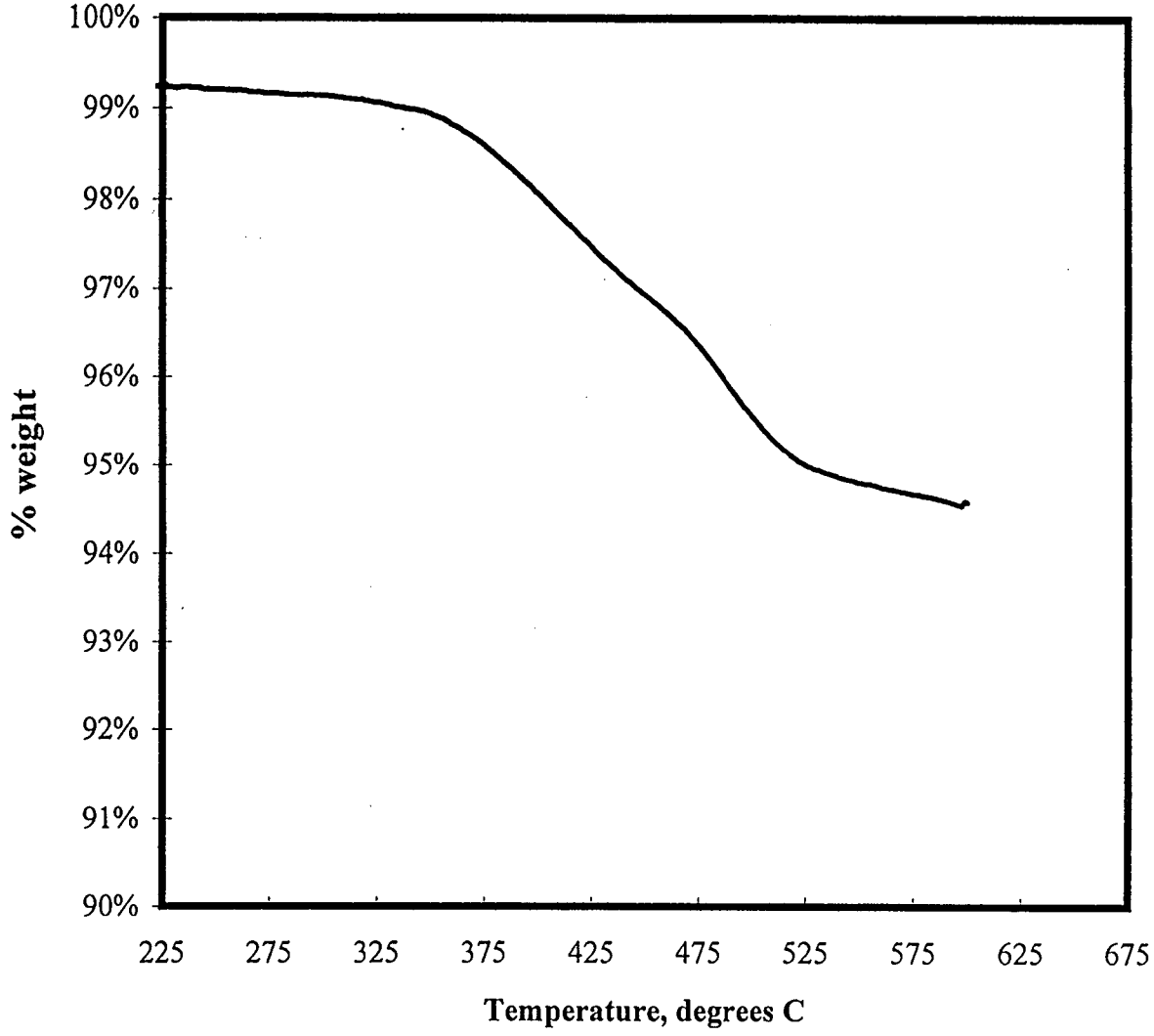
100%
99%
98%
97%
96%
95%
94%
93%
92%
91%
90%
% weight
225
275
325
375
425
475
525
575
625
675
Temperature, degrees C

Figure 5

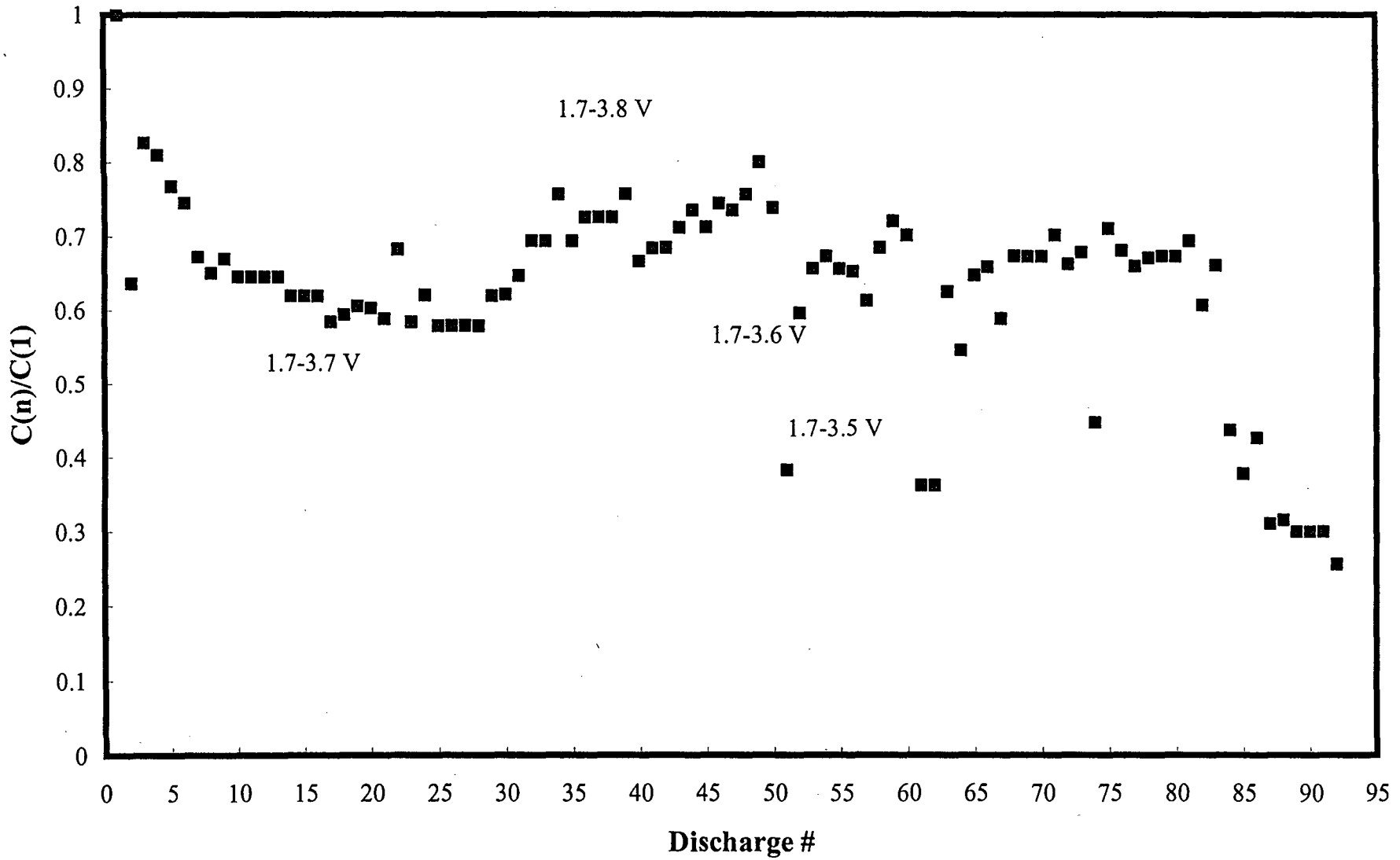
1.7-3.8 V
1.7-3.7 V
1.7-3.6 V
1.7-3.5 V
C(n)/C(1)
Discharge #
0
0.1
0.2
0.3
0.4
0.5
0.6
0.7
0.8
0.9
1
0
5
10
15
20
25
30
35
40
45
50
55
60
65
70
75
80
85
90
95

Figure 6

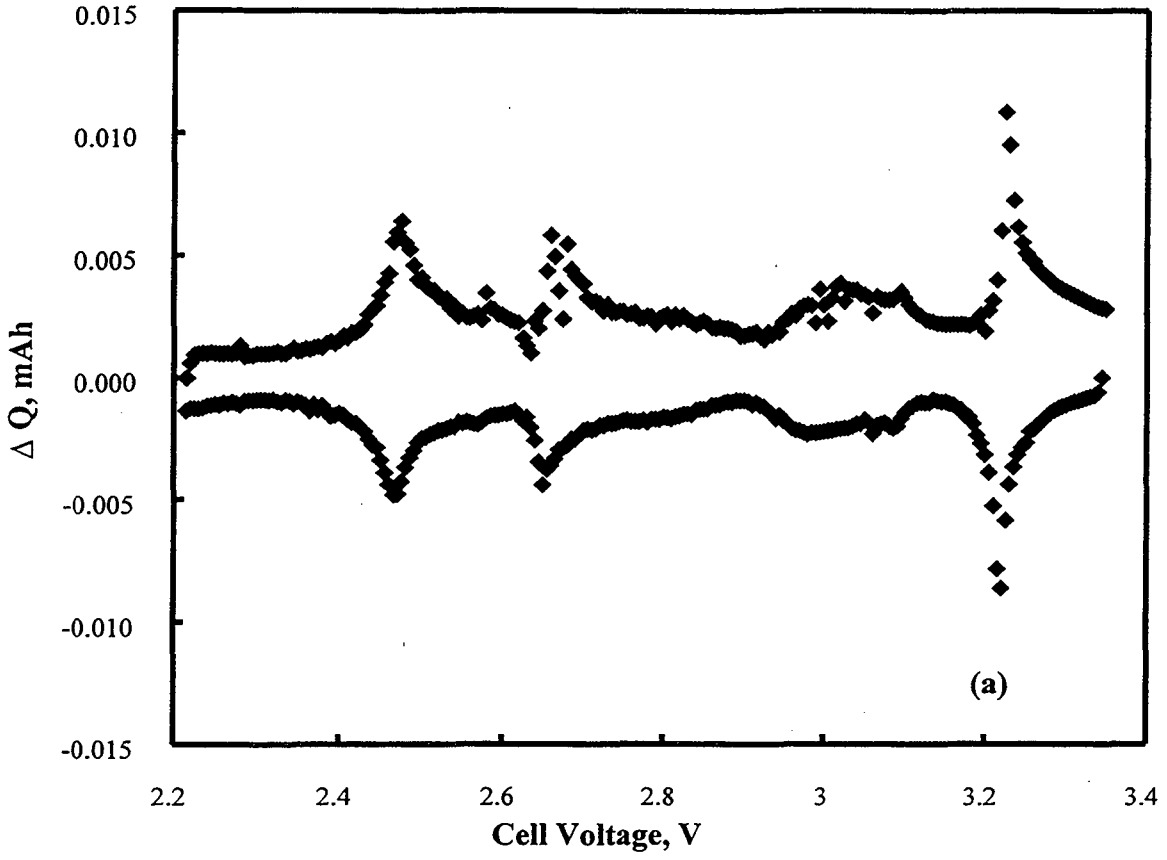
0.015
0.010
0.005
0.000
-0.005
-0.010
-0.015
Δ Q, mAh
(a)
2.2
2.4
2.6
2.8
3
3.2
3.4
Cell Voltage, V

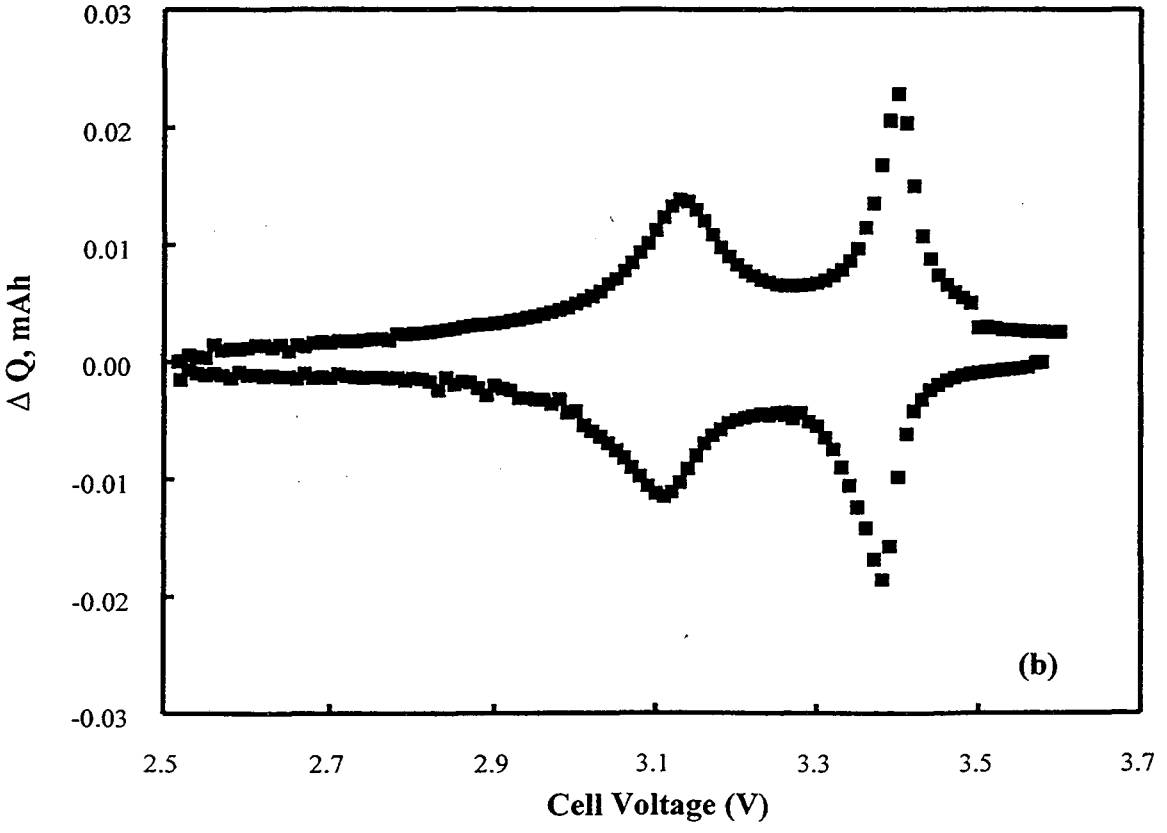
0.03
0.02
0.01
0.00
-0.01
-0.02
-0.03
Δ Q, mAh
(b)
2.5
2.7
2.9
3.1
3.3
3.5
3.7
Cell Voltage (V)

Figure 7

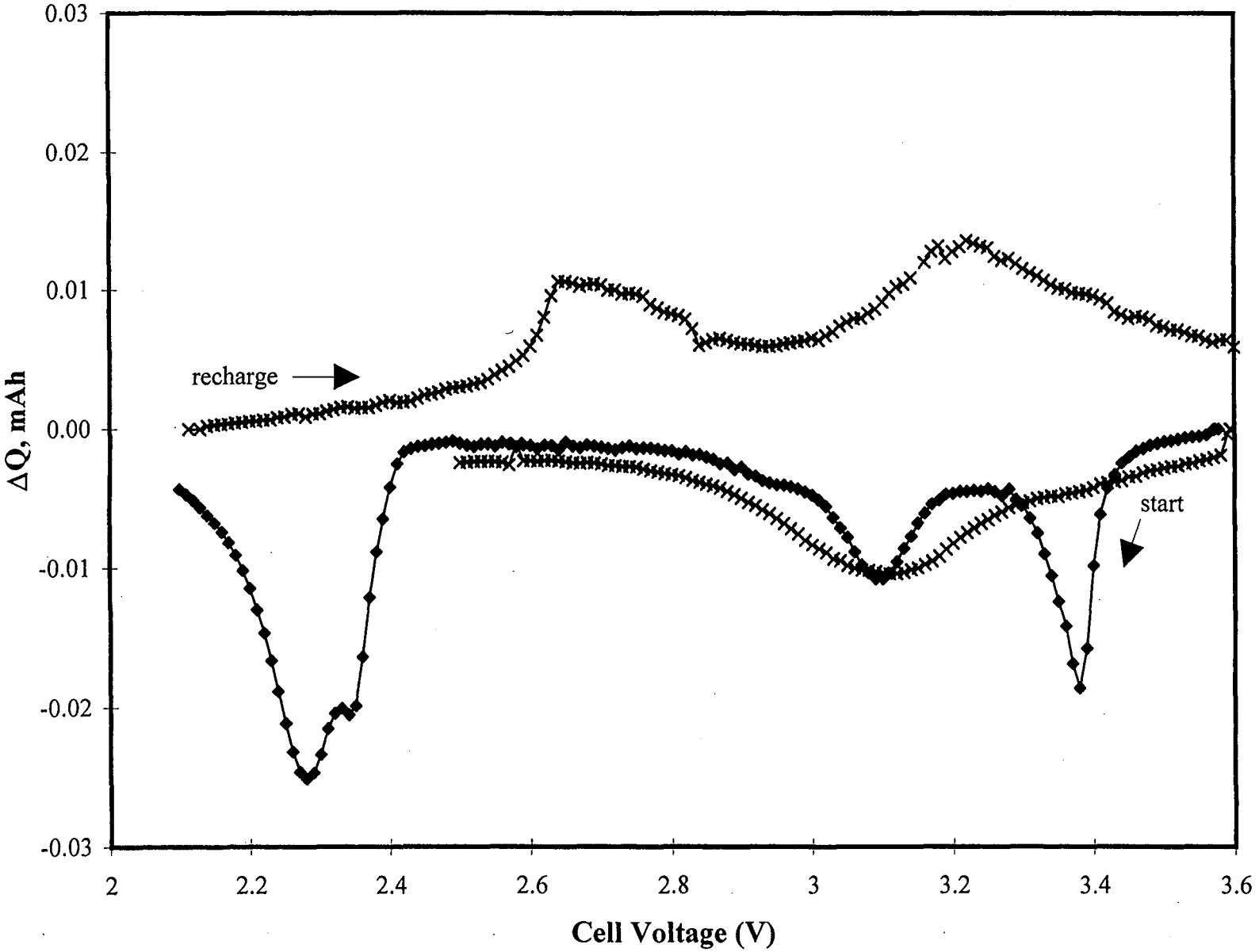
0.03
0.02
0.01
0.00
-0.01
-0.02
-0.03
ΔQ, mAh
recharge
start
2
2.2
2.4
2.6
2.8
3
3.2
3.4
3.6
Cell Voltage (V)

Figure 8

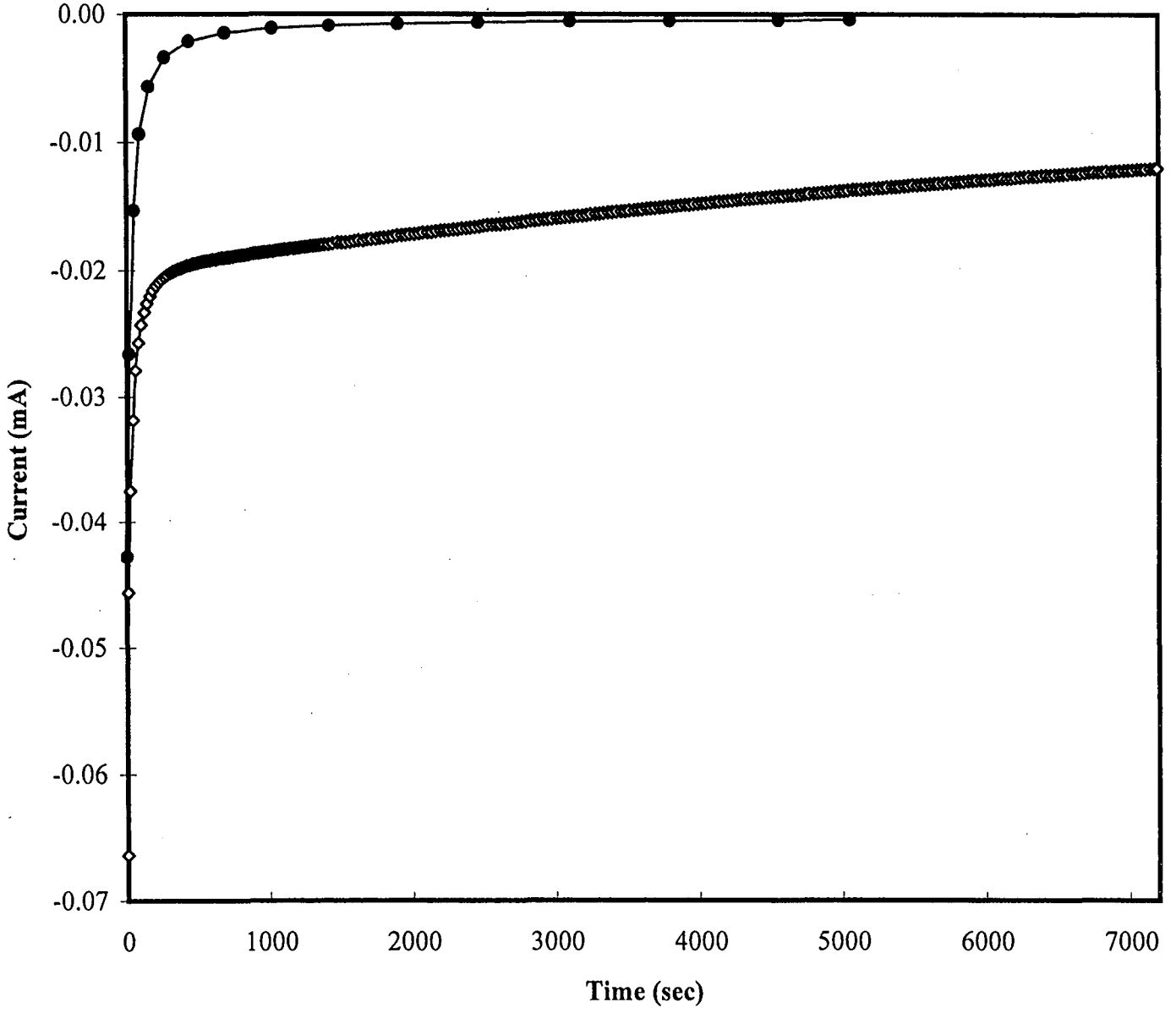
0.00
-0.01
-0.02
-0.03
-0.04
-0.05
-0.06
-0.07
Current (mA)
0
1000
2000
3000
4000
5000
6000
7000
Time (sec)

Figure 9

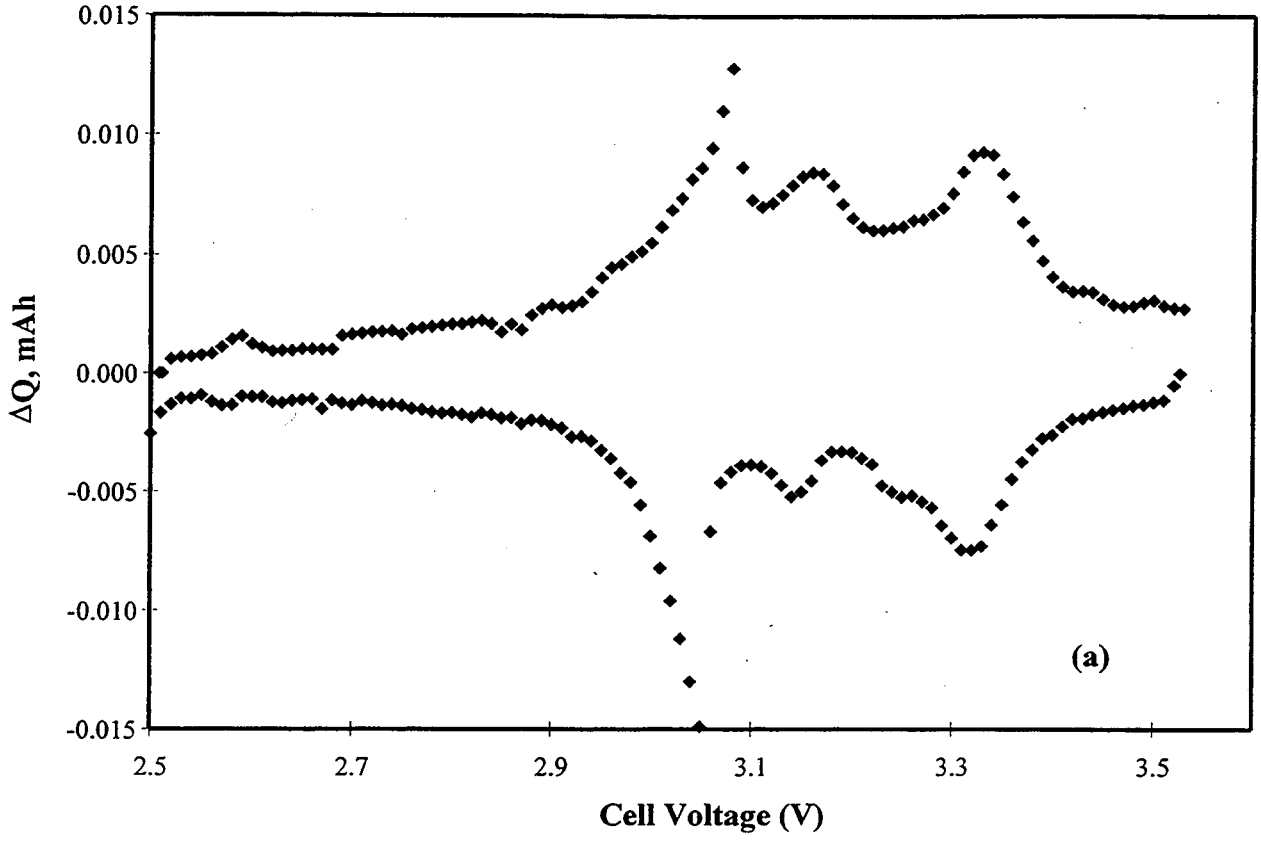
0.015
0.010
0.005
0.000
-0.005
-0.010
-0.015
ΔQ, mAh
(a)
2.5
2.7
2.9
3.1
3.3
3.5
Cell Voltage (V)

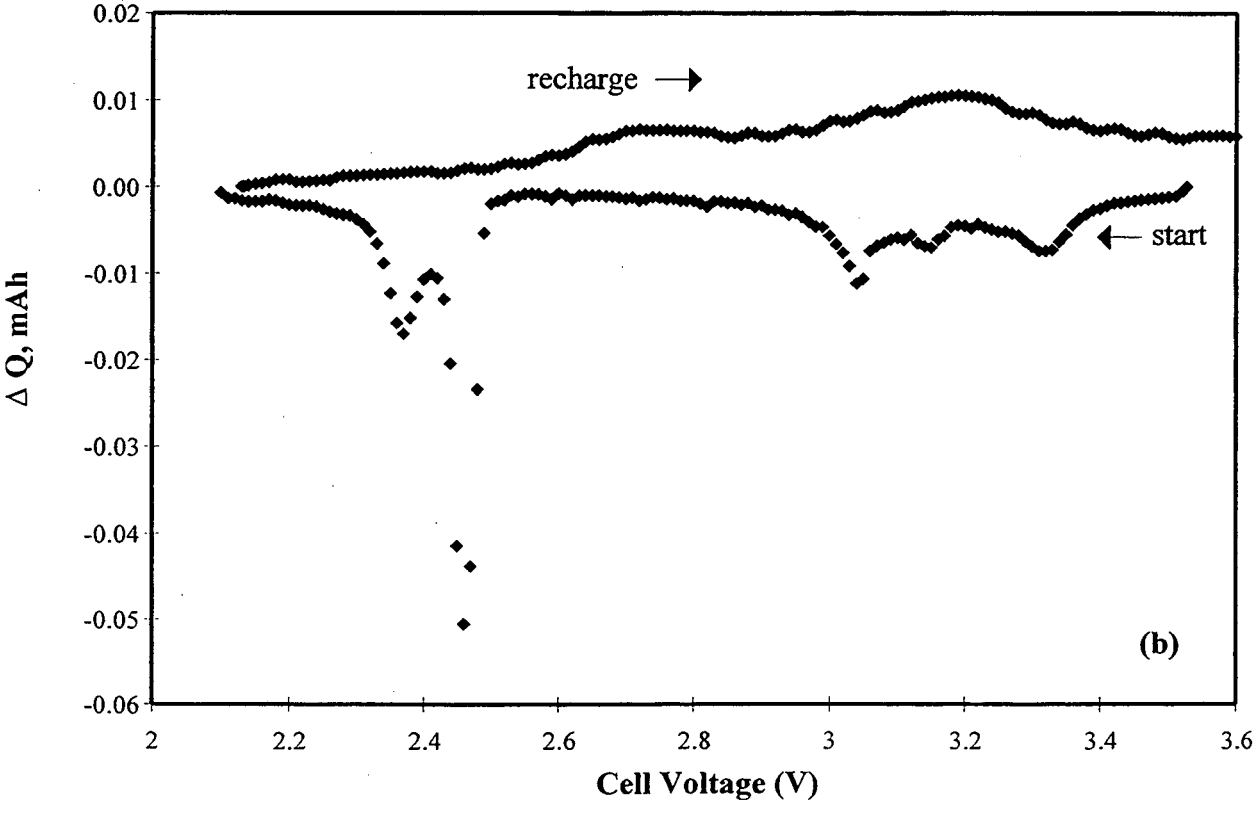
0.02
0.01
0.00
-0.01
-0.02
-0.03
-0.04
-0.05
-0.06
Δ Q, mAh
recharge
start
(b)
2
2.2
2.4
2.6
2.8
3
3.2
3.4
3.6
Cell Voltage (V)

Figure 10

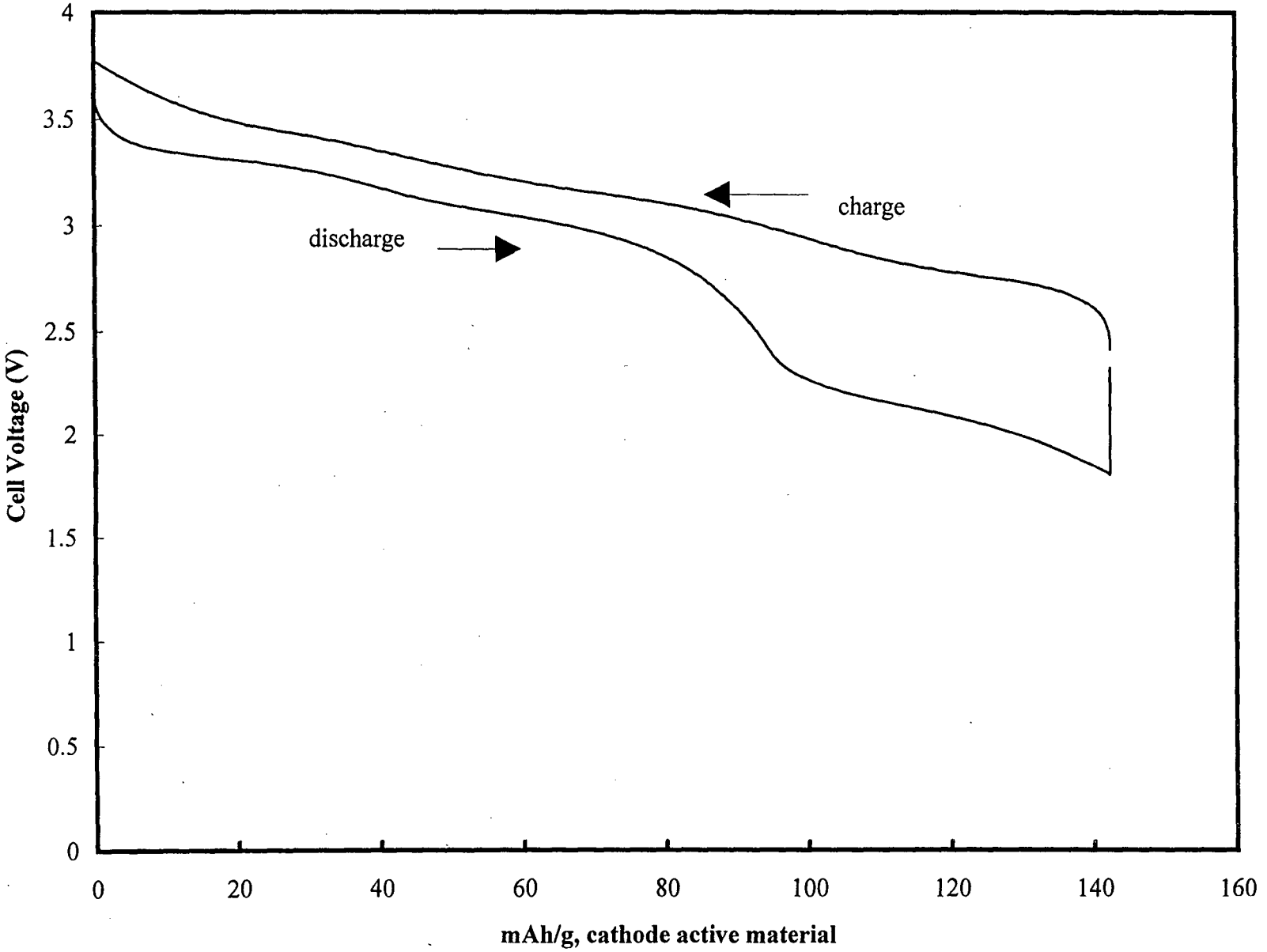
4
3.5
3
2.5
2
1.5
1
0.5
0
Cell Voltage (V)
charge
discharge
0
20
40
60
80
100
120
140
160
mAh/g, cathode active material

Figure 11

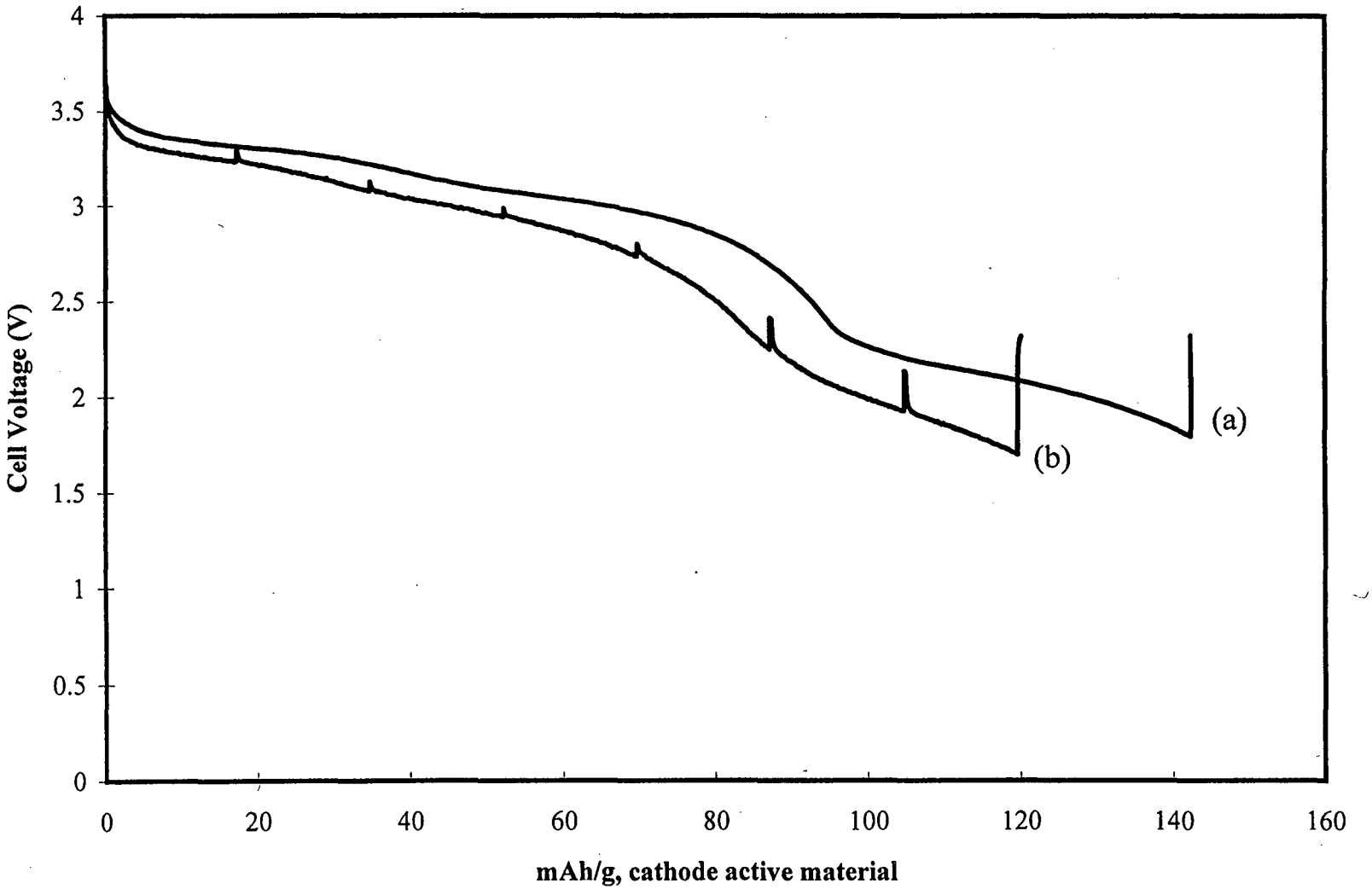
Cell Voltage (V)
4
3.5
3
2.5
2
1.5
1
0.5
0
0
20
40
60
80
100
120
140
160
mAh/g, cathode active material
(a)
(b)

Figure 12

LAWRENCE BERKELEY LABORATORY
UNIVERSITY OF CALIFORNIA
TECHNICAL INFORMATION DEPARTMENT
BERKELEY, CALIFORNIA 94720